Research article

JGS
Journal of the Geological Society

https://doi.org/10.1144/jgs2024-031 | Vol. 181 | 2024 | jgs2024-031

The interplay of lithology, tectonics and climate in the morphology of Corsica

Rebekah M. Harries[1], Chrystiann Lavarini[2], Linda A. Kirstein[2*], Mikael Attal[3] and Simon M. Mudd[3]

[1] Institute of Hazard, Risk and Resilience, Durham University, Lower Mount Joy, South Road, Durham DH1 3LE, UK
[2] Grant Institute, School of GeoSciences, University of Edinburgh, The King's Buildings, James Hutton Road, Edinburgh EH9 3FE, UK
[3] Institute of Geography, School of GeoSciences, University of Edinburgh, Drummond Street, Edinburgh EH8 9XP, UK
LAK, 0000-0001-5496-4081
*Correspondence: linda.kirstein@ed.ac.uk

Abstract: The morphology of the landscape on the island of Corsica in the western Mediterranean Sea is transient with a clear topographic asymmetry. The geology of the island can be divided into two units – Hercynian Corsica and Alpine Corsica – with contrasting lithology, climate and structural controls between them. We used topographic analysis to assess the influence of each of these factors on landscape form. Disequilibrium in the landscape is illustrated by analysing χ and Gilbert metrics, which indicate active migration of the drainage divide, along with a new metric that quantifies tributary heights above the main stem channel. The climate in the region has fluctuated dramatically from the Messinian salinity crisis through to Quaternary glaciation. However, analysis of the size and distribution of knickpoints across the island does not reflect specific base-level changes. Instead, the basement structures control valley orientation and the conditioning of the landscape by glaciation exerts strong controls on drainage evolution.

Supplementary material: Drainage divide stability metrics for χ, relief, gradient and elevation collected from the channel heads, and differences in elevation of tributaries and main stem channels for Corsica calculated using χ Q are available at https://doi.org/10.6084/m9.figshare.c.7278131

Received 13 February 2024; **revised** 21 May 2024; **accepted** 31 May 2024

There is still some debate regarding the relative controls exerted by lithology, tectonics and climate on the development of topography and on the topographic response to changes in boundary conditions (Whipple 2001; Mudd 2017). Studies integrating the analysis of various parts of the landscape offer the best opportunity to disentangle such controls because river profiles, hillslopes and drainage divides are expected to respond differently to different forcings. For example, river profiles and hillslopes record changes in erosion, exhumation and uplift rates over a range of short to long timescales (10^4 to 10^7 years) (Whipple 2001; Finnegan *et al.* 2014; Kirstein *et al.* 2014; Mudd 2017). River steepness has been used as a proxy for inferring spatial changes in rock uplift and erodibility, whereas breaks in channel slope (knickpoints) have been used to infer temporal and spatial changes in erosion in response to varying environmental conditions (e.g. erodibility, structural boundaries and uplift) (Crosby and Whipple 2006; Baynes *et al.* 2015; Brocard *et al.* 2016). On shorter timescales (<10^4 years) different parts of the geomorphic system may be responding to different forcings at different times – for example, base-level changes coupled with glaciation should result in complex adjustment signals in downstream and upstream catchment areas, respectively (Harries *et al.* 2023).

Corsica is an ideal location in which to study the interplay between tectonics, erosion and climate (Fig. 1). This mountainous island has experienced exhumation rates of 25–220 mm kyr^{-1} since the late Miocene and erosion rates of similar magnitude over the Quaternary (Fellin *et al.* 2005*a*, *b*; Kuhlemann *et al.* 2007, 2009; Sømme *et al.* 2011; Molliex *et al.* 2017). With a maximum elevation of 2706 m, the high summits of Corsica experienced glaciation during the last glacial maximum (Kuhlemann *et al.* 2005) (Fig. 2). A precipitation gradient exists across the island (Kuhlemann *et al.* 2005; Fick and Hijmans 2017) (Fig. 2). Importantly, the bulk of the island is made of a north–south elongated Hercynian basement block (mostly granitoids and associated felsic volcanic rocks) that encompasses the highest summits and the main north–south drainage divide (Figs 1, 3). To the NE, this basement block is flanked by a slab of Alpine units (mostly flysch and ophiolite) (Fig. 3), which has the effect of lengthening the eastward draining rivers. Corsica's topography also reveals an asymmetry of the main drainage divide, which is located to the west of the central axis of Hercynian Corsica to the north, whereas it is to the east of this axis in the south (Fig. 1). This curious divide configuration raises questions about its origin and if it may be caused by temporally variable climate and/or tectonic forcings.

The modern topography of Corsica features lithological variability, precipitation gradients and recent glaciation, all of which are superimposed on an active tectonic legacy. Our aim is to disentangle these factors to understand why the morphology of the northern part of the island is fundamentally different from that of the south of the island. We analyse channel longitudinal profiles, identify breaks in slope (i.e. knickpoints) and quantify topographic proxies for the stability of drainage divides and hillslopes. We also develop a new method that quantifies the difference in elevation between tributary sources and the main channels to illustrate over-deepening of either the tributaries or the main stem. Combined, these approaches allow us to test whether transient signals can be identified and to assess the degree of sensitivity of the landscape in adapting to external forcing. The insights gained should be applicable to evaluating other high-relief, post-glacial landscapes around the globe.

Study area

Corsica is the fourth largest island in the Mediterranean Sea and has a number of mountain peaks >2000 m in elevation (Fig. 2). East–

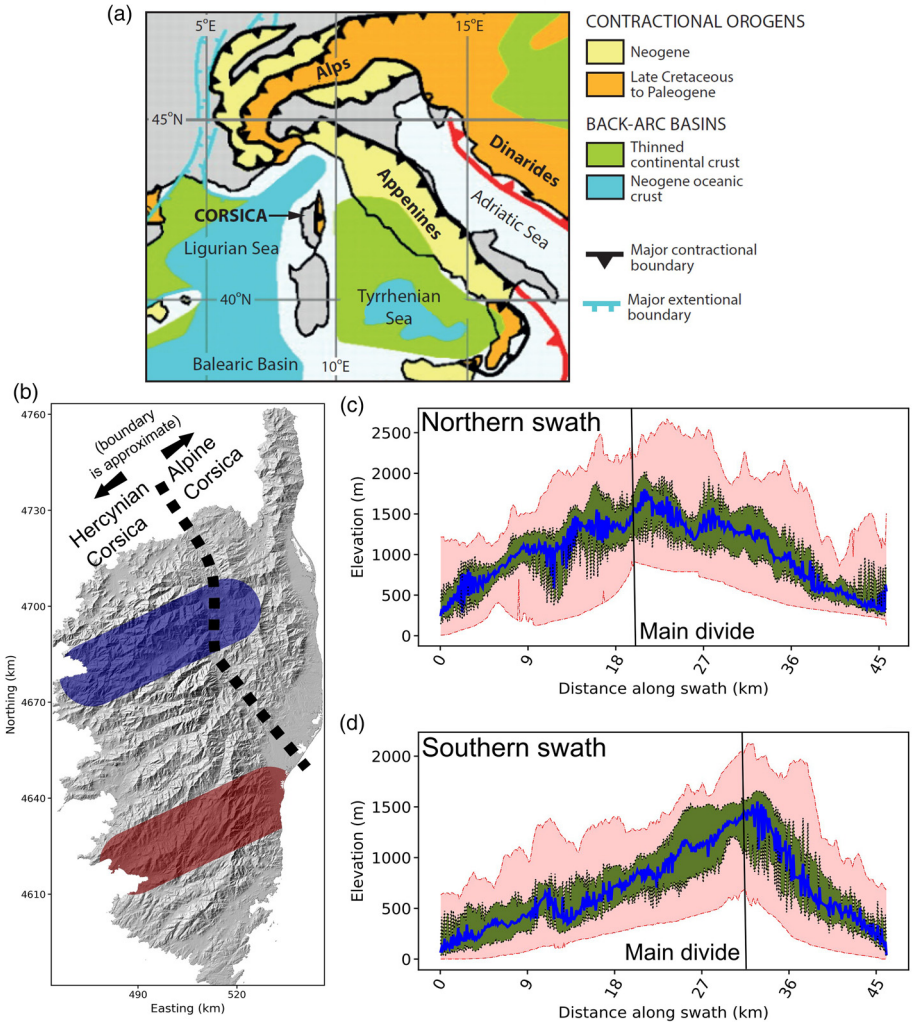

Fig. 1. (**a**) Location of Corsica within the western Mediterranean domain. (**b**) Hillshade view of Corsica highlighting the locations of the two swath profiles (**c**, **d**) from the northern and southern sections of Hercynian Corsica. The lower line on the swath profile is the minimum elevation within the swath and roughly tracks the channel elevation. This is used to delineate the drainage divide. The dark blue line is the median elevation, the green area brackets the 25th and 75th percentiles of elevation and the top line is the maximum elevation in the swath. Source: part (a) adapted from Platt (2007).

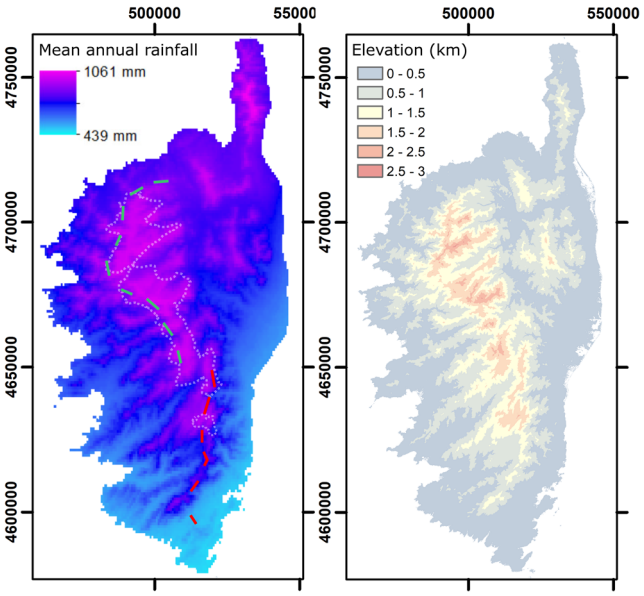

Fig. 2. Left-hand panel: spatial distribution of the mean annual rainfall across Corsica derived from Worldclim climate data for the time period 1970–2000 (Fick and Hijmans 2017). The dotted white line is the extent of glaciation at the last glacial maximum (after Kuhlemann *et al.* 2005). Right-hand panel: variation in elevation on Corsica colour-coded for 500 m intervals. Notice that higher elevation is focused to the west in northern Corsica.

west, across the island's 83 km width, there are dramatic changes in the total relief and large cut-and-fill Quaternary river terraces, which indicate landscape transience. The mountain relief increases from south to north, which may be partially related to its tectonic history. In the south, the minimum elevation varies from sea-level to *c.* 650 m, while the maximum elevation along the indicative 45 km swath profile is *c.* 2200 m (Fig. 1). This is in contrast with the north, where the minimum elevation changes from sea-level to 1100 m and the maximum elevations are >2600 m (Fig. 1). The form and location of the drainage divide are distinctly different between the south and the north. The drainage divide is asymmetrical and is located further east in the south, with noticeably greater elevation (and steeper relief to the east) (Fig. 2).

The NE of the island, known as Alpine Corsica, was accreted during Alpine orogenesis from *c.* 65 to 34 Ma, when oceanic and transitional crust was obducted onto Hercynian Corsica, which makes up the rest of the island (Turco *et al.* 2012). As a result, there are contrasting lithological and structural controls between Hercynian and Alpine Corsica (Fig. 3). The high relief, however, may also be related to the lithology, climate gradients and the pre-existing geological structures being exploited by river systems.

Topographic and geological development of the study area

Corsica contains two main geological units: Hercynian and Alpine Corsica (Figs 1, 3). Hercynian Corsica consists of three lithological units that cover the majority of the island's onshore area (Rossi *et al.* 1994) (Fig. 3). These units include unmetamorphosed

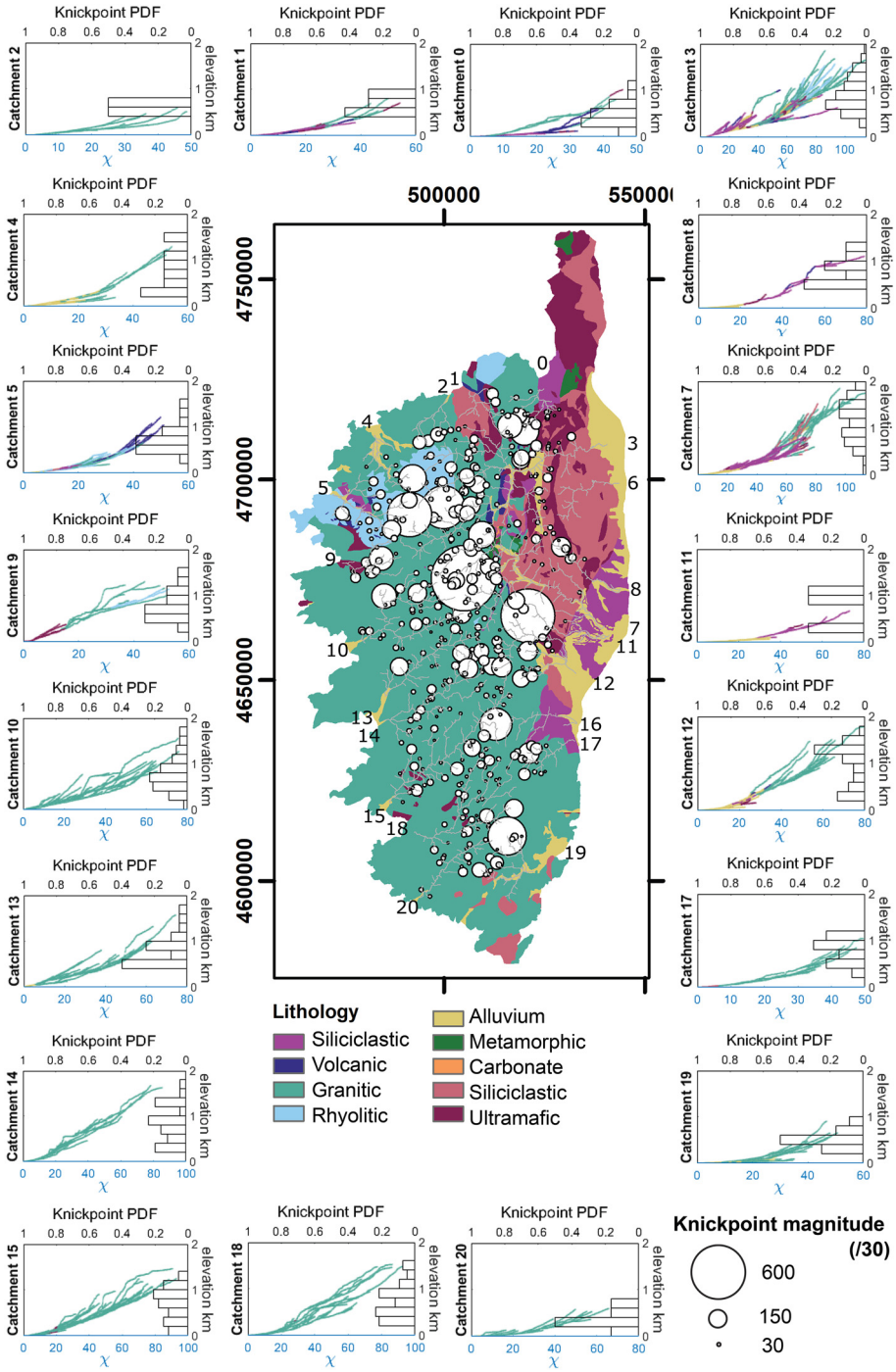

Fig. 3. Overview of the basic geology of Corsica and the form of the main stem and contributing tributaries for each catchment (labelled 0–20), and the location and magnitude of knickpoints (white circles). Probability density function (PDF) with histograms showing the relative abundance of knickpoints per 200 m elevation interval. The knickpoint magnitude is divided by 30 to visualize effectively at map scale.

Carboniferous–Early Permian granitoids, Permian volcanic rocks and gneiss, partly overlain by continental and marine sedimentary rocks (Triassic–Paleocene) and by Eocene foredeep strata that are strongly deformed (Fig. 3). The basement fabric, with a widely spaced fault pattern, determines the SW–NE-oriented catchments of western Corsica (Fig. 4). Alpine Corsica includes metamorphosed oceanic rocks thrust on top of Eocene foredeep strata and Hercynian basement overlain by Miocene–Pliocene sediments (Fig. 3). Thick accumulations of Miocene–Pliocene sediments are located in the east and NE, forming the sedimentary plains of Marama and Aleria (Fig. 3).

Corsica experienced protracted exhumation from Mesozoic to Cenozoic times, culminating in the late Miocene following the accretion of an Alpine terrane to Hercynian Corsica (Fellin *et al.* 2005*a*, *b*). Apatite fission track and apatite (U–Th)/He dating reveal cooling ages that suggest Cenozoic (40–14 Ma) asymmetrical exhumation of Corsica from south to north (Cavazza *et al.* 2001; Fellin *et al.* 2005*a*, *b*; Danišík *et al.* 2007). Exhumation started in the south of Corsica in the Late Oligocene (40–30 Ma) and propagated northward through early Miocene times, reaching the centre at 30–20 Ma and the northern region at 20–17 Ma (Danišík *et al.* 2007). The island is considered to be at, or approaching, an exhumational steady-state today (Molliex *et al.* 2017).

High uplift rates (1.5 km Myr^{-1}) are recorded from mid-Miocene (*c.* 14 Ma) times, with evidence of drainage reorganization in the north of Corsica (Fellin *et al.* 2005*b*; Cavazza *et al.* 2007). In the large Golo River watershed (catchment 3, Fig. 3), apatite (U–Th)/He dating provides a long-term exhumation rate of 25–220 mm kyr^{-1} over the last 7–3 Ma (Fellin *et al.* 2005*b*; Kuhlemann *et al.* 2009).

Published Quaternary erosion rates vary from 15 to 420 mm kyr^{-1} (similar to long-term estimates), with variability depending on

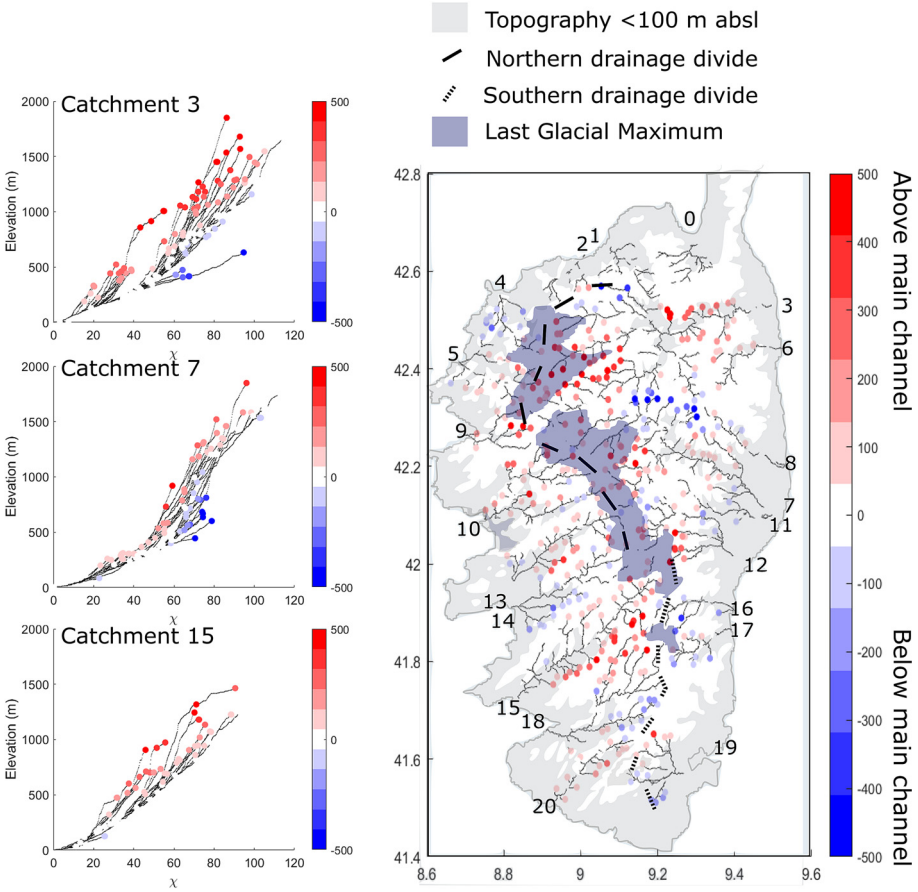

Fig. 4. Difference in elevation of the tributaries and their main channels at the same χ-distance upstream. Left-hand panels: the χ-elevation profiles of three catchments located on the eastern (catchments 3 and 7) and western (catchment 15) sides of the drainage divide. Each tributary's source point is coloured according to its elevation above the main channel in χ-space. Right-hand panel: the tributary sources are plotted in plan-view on top of Corsica's river network. The extent of glaciation at the last glacial maximum and mapped faults are also included to give tectonic and glacial context.

geographical location and the technique applied – for example, lower erosion rates are estimated from detrital ^{10}Be (Kuhlemann *et al.* 2007, 2009; Sømme *et al.* 2011; Molliex *et al.* 2017). Incision rates estimated from river terraces by optically stimulated luminescence for the Golo River range from 190 to 420 mm kyr^{-1}, with values varying between the different tectonic domains of Hercynian and Alpine Corsica (Sømme *et al.* 2011). Based on seismic reflection profiles and the analysis of offshore basins, Calvès *et al.* (2013) found catchment-wide erosion rates of 47–219 mm kyr^{-1} for the last 130 ka, whereas Molliex *et al.* (2017) estimated short-term erosion rates of 15–95 mm kyr^{-1} using detrital ^{10}Be cosmogenic nuclides. In the Tavignano River watershed (catchment 7, Fig. 3), Molliex *et al.* (2017) measured catchment-wide erosion rates of 40–74 mm kyr^{-1}.

These catchment-wide erosion rates are much lower than the incision rates (160–475 mm kyr^{-1}) of the Golo River (Fellin *et al.* 2005*b*; Sømme *et al.* 2011). Although there is no short-term catchment-wide erosion rate available to directly compare both sides of the drainage divide, studies conducted by Kuhlemann *et al.* (2007, 2009) indicate that erosion rates are low at the mountain summits (Kuhlemann *et al.* 2009). There is a clear spatial variation in the measured erosion rates at the mountain summits in northern Corsica, with a westward increase from 9.1 mm kyr^{-1} (east) to 13.6 mm kyr^{-1} (centre) to 17.6 mm kyr^{-1} (west) (Kuhlemann *et al.* 2009). These erosion rates correlate with modern annual precipitation rates, which are higher on the western side of the Corsican drainage divide, suggesting a potential climatic influence.

Corsica is located both north and west of active plate boundaries in the Mediterranean region (Fig. 1). Seismic activity in the Corsica–Sardinia region is sporadic, as indicated by the CTPI15 earthquake catalogue (Rovida *et al.* 2020). Available GPS measurements in the region indicate that the GPS velocity is <0.5 mm a^{-1}, with a weak horizontal velocity field (Devoti *et al.* 2017). Neotectonic activity in the region is limited.

Sea-level and climate

Corsica's position in the western Mediterranean Sea means it retains an excellent record of climate change since the Pliocene. The Messinian crisis affected the Mediterranean region during the late Miocene (Gargani 2004). The first phase of drying out at *c.* 5.9 Ma lasted for *c.* 400 kyr and resulted in 600–700 m of sea-level fall at an average rate of *c.* 1.45 mm a^{-1}. The second phase of drying out at *c.* 5.5 Ma was marked by a drop of 1300–1700 m in sea-level over 50 kyr (30 mm a^{-1}). The crisis ended at *c.* 5.3 Ma (Gargani 2004). More modest, yet significant, sea-level variations occurred over the Quaternary, associated with successive glacial and interglacial periods. Waelbroeck *et al.* (2002) proposed that, in the last 130 ka, the sea-level in the Mediterranean experienced a steady lowering of 120 m between 130 and 20 ka (1.1 mm a^{-1}), followed by a rise to the present level at a rate of *c.* 6 mm a^{-1}. Changes in base-level should, in theory, propagate upstream in drainage networks, resulting in the development of transient knickpoints. The rate at which this occurs is expected to depend on the rock strength (e.g. Niemann *et al.* 2001; Zondervan *et al.* 2020); however, given that calc-alkaline granites dominate Hercynian Corsica (Fig. 3), any differences in rock strength should be minimal.

In the Quaternary, the southern region of the island experienced periglacial activity and glaciers were absent. The northern and central mountains of Hercynian Corsica were strongly glaciated during the Würmian, which ended 11 700 years ago, while Alpine Corsica was unglaciated (Kuhlemann *et al.* 2005) (Fig. 2). Glaciers reached their maximum extent *c.* 18 kyr ago in the centre and northwestern sections of Corsica, extending down to 500 m a.s.l. (Kuhlemann *et al.* 2005). Remnants of this extensive glaciation include over-deepened valleys, glacial lakes and cirques, which can be made out in the hillshade in Figure 1.

Today, Corsica is free of permanent ice and experiences a subtropical Mediterranean climate with temperate wet winters and

warm, dry summers. The mean annual rainfall varies from *c.* 439 mm in the south to 1061 mm in the NW (Fig. 2). The northeastern parts of the mountain range are drier than the central and southern parts, resulting in an asymmetrical precipitation pattern (Fig. 2). The current drainage divide is located within the region of the north that was most affected by glaciation (Fig. 2).

Here, we explore the stability of the Corsica drainage divide and argue that the landscape has been pre-conditioned by both early tectonic activity (fault development) in the south and climate (glacial over-deepening) in the north, leading to the migration of the drainage divide to the west in the south and to the east in the north.

Methods

To analyse the geomorphology of our study area, we deployed a number of topographic metrics designed to identify areas of heterogeneity in erosion rates or lithology, as well as metrics thought to indicate the stability of the drainage divide. Gilbert (1877) reasoned that steeper channels should erode faster than gentle ones, all else being equal, but a confounding factor is that the channel gradient is strongly correlated with the drainage area (Morisawa 1962). Building on the work of Morisawa (1962), Flint (1974) formalized a power law relationship between the gradient and drainage area:

$$S = k_s A^{-\theta} \tag{1}$$

where the parameter k_s is defined as the steepness index and θ is defined as the concavity index. Subsequent work has shown that the steepness index correlates closely with the erosion rate (e.g. Kirby and Whipple 2012). To calculate k_s, we first transformed the channel profile by integrating the drainage area along the channel (e.g. Perron and Royden 2013):

$$\chi = \int_{x_b}^{x} \left(\frac{A_0}{A(x)} \right)^{\theta} \mathrm{d}_x \tag{2}$$

where χ is a longitudinal coordinate in units of metres, A_0 is an arbitrary scaling drainage area and x is the non-transformed long profile distance in meters and x_b is the distance where integration starts (with the subscript b denotating base level). When $A_0 = 1\ \mathrm{m}^2$, the gradient $\mathrm{d}z/\mathrm{d}\chi$ is equal to the steepness index k_s (e.g. Goren *et al.* 2014; Mudd *et al.* 2014).

Both the coordinate χ and the steepness index k_s depend on the value of the concavity index θ. To make comparisons between different basins, a reference value of the concavity index, θ_{ref}, is frequently used (Wobus *et al.* 2006*a*). Once applied, the steepness indices derived using this reference concavity are referred to as the normalized steepness index, k_{sn}.

Various methods have been proposed to calculate the most likely value of θ for a given drainage basin, but Mudd *et al.* (2018) found that a method based on the relative disorder of χ-elevation profiles (Goren *et al.* 2014) was the most resilient to tectonic and lithological heterogeneity. After performing a disorder analysis, we selected a θ_{ref} value of 0.35.

We investigate the north–south regional drainage divide of Corsica using both χ and Gilbert metric analyses. Willett *et al.* (2014) proposed that differences in χ across divides were indicators of divide migration, with divides moving away from the side with lower values of χ. However, the choice of base-level for the integration, as well as spatial variations in erodibility, Hack's coefficient and channel tortuosity, can significantly affect the χ-values of rivers at divides (Whipple *et al.* 2017; Forte and Whipple 2018; Zhou *et al.* 2022*a*, *b*), so coupling χ analyses with Gilbert metrics is thought to be more robust. Gilbert metrics represent a top-down assessment of landscape stability, similar to the analysis of channel head segments and the cross-divide contrast index recently developed by Zhou and co-workers, which also offers the possibility of identifying uplift gradients and calculating the migration rates of drainage divides (Zhou *et al.* 2022*a*, *b*, 2024; Zhou and Tan 2023). Morphometric parameters, including the upstream gradient, relief and the elevation at the channel heads, are expected to vary with short-term erosion rates (10^3–10^5 years) and therefore indicate disequilibrium, as suggested by Gilbert (1877) and Forte and Whipple (2018).

We used SRTM topographic data with a pixel size of *c.* 30 m and set a threshold for initiating a channel at 2500 pixels (corresponding to a drainage area >2.25 km^2). We then calculated the channel gradient at these source points, averaged over a 10 m drop in elevation, as suggested by Wobus *et al.* (2006*a*), and compared the difference in the gradient across the divide. The gradient asymmetry across the divide is one of the four Gilbert metrics described by Forte and Whipple (2018), although we note that, in their work, the gradient is averaged from the channel head to the divide. We prefer using the gradient local to the channel head because the gradient from the channel head to the divide can be sensitive to the hillslope length (e.g. Grieve *et al.* 2016). Steeper gradients in the same drainage area (in this case, the drainage area at a fixed number of pixels) should result in faster erosion, all else being equal, so the divide should migrate away from the steeper channel.

We located knickpoints along the channel networks. Knickpoints are local steepenings in the channel profiles, identified by changes in k_{sn}. These features could be related to changes in the underlying channel erodibility (e.g. Duvall *et al.* 2004) or could be indicative of a change in the erosion rate (e.g. Knopf 1924). Knickpoints that originate from base-level changes (e.g. changes in sea-level) or differential changes in the uplift rates (e.g. from increased fault activity) will migrate upstream (e.g. Knopf 1924). Royden and Perron (2013) demonstrated that knickpoints originating from a common base-level across a landscape with homogenous uplift and substrate should share the same χ-coordinate.

We obtained the locations of all knickpoints in our study area by first segmenting the channel network into reaches with similar gradients in the χ-elevation space using the statistical method of Mudd *et al.* (2014). This results in data about this gradient (which is equal to k_{sn}) as a function of χ. We followed the method of Gailleton *et al.* (2019) to first denoise the data, combine nearby knickpoints and then select the largest knickpoints as judged by the change in the channel steepness index. The 'magnitude' of the knickpoint is defined by the change in k_{sn} (Δk_{sn}) across the knickpoint. Denoising is performed on the along-channel k_{sn} values using a total variation denoising filter (Condat 2013), with a parameter that controls the amount of denoising, l, which has been tuned to the concavity index based on the sensitivity analysis of Gailleton *et al.* (2019). Knickpoints are combined if they are within ten pixels of each other (i.e. two knickpoints with the same Δk_{sn} within a ten-pixel window will lead to a combined knickpoint double the value of Δk_{sn} compared with one of the original knickpoints). We then thinned the dataset (because there are many small changes in k_{sn}) by retaining the largest (by magnitude) 20% of knickpoints. We plotted knickpoint locations in conjunction with lithology of the channel bed to differentiate between the knickpoints generated by lithological contrasts from those that cannot be explained by the lithology (Fig. 3).

We then introduced a new metric designed to highlight the presence of hanging tributaries. Hanging tributaries are frequently found in glaciated landscapes and are thought to be caused by differential erosion by glaciers in the main valley and tributaries (e.g. Penck 1905). Hanging valleys may also be caused by incision in the main channel that exceeds an erosion threshold in the tributaries (e.g. Wobus *et al.* 2006*b*). In the former case, hanging valleys will be limited to the glaciated parts of the landscape, whereas, in the latter, hanging valleys will be

located downstream of major incision pulses (i.e. downstream of the knickpoints). Lithological variations may also lead to hanging valleys – for example, in a situation where a main stem channel exploits a weak lithology, this should lead to patterns of tributary heights above the main stem that are distinct from the other scenarios described here.

In a landscape without hanging valleys, tributaries at the same χ-coordinate as the main stem channel should share the same elevation (Royden and Perron 2013). A hanging valley will therefore have a higher elevation than the main stem channel at the same χ-coordinate. We reason that this difference will be most easy to identify at the tributary sources because they will be upstream of the hanging section, if one exists. We therefore extracted the χ-coordinate of all tributary sources and compared the elevation of these sources with the elevation of the main stem channel at the same χ-coordinate. We note that this metric will be highly sensitive to the θ_{ref} value used in the analysis, which is a limitation. We highlight the importance of using a θ_{ref} value that minimizes the relative disorder of χ-elevation profiles rather than maximizing the linearity of profiles because such a method was shown to perform best when recovering the θ_{ref} value from simulated topographies in landscapes with non-uniform lithologies and uplift (Mudd *et al.* 2018).

Results

Drainage divide stability

The regional drainage divide is segmented in two parts (A and B), where a distinct contrast is observed in both χ and the Gilbert gradient metric (Fig. 5). The southern section of the Corsica drainage divide (A) is marked by values of χ and differences in channel gradient that suggest a westward divide migration trend (i.e. the eastward-flowing rivers have lower χ and higher gradient and relief values closer to the divide than the westward-flowing rivers) (Fig. 5, Supplementary Figure S1). However, the northern section of the drainage divide (B) highlights an eastward divide migration trend (i.e. the westward-flowing rivers have lower χ and higher gradient and relief values closer to the divide than the eastward-flowing rivers) (Fig. 5, Supplementary Figure S1).

Spatial distribution and dimensions of knickpoints

The occurrence of knickpoints shows an interesting spatial distribution with respect to tectonic structures and the extent of Würmian glaciation (Figs 3, 4). Migrating knickpoints can be generated by base-level changes or differential uplift at faults. Base-level changes derived from changing sea-levels would result in the

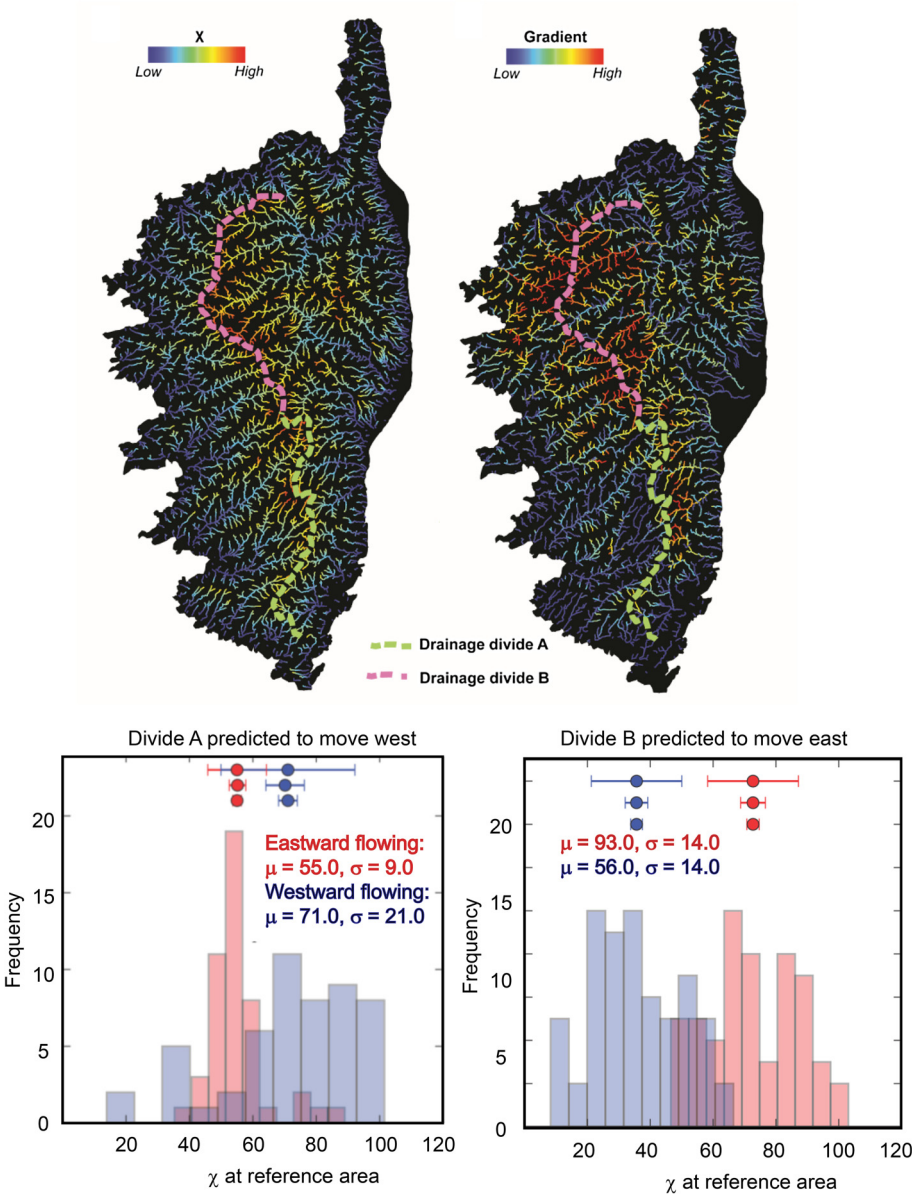

Fig. 5. The χ-values (left) and normalized values of the upstream gradient (right) of the drainage network across Corsica. The regional drainage divide was segmented into two shorter divides (A, south; and B, north) based on the visual anomaly in χ and the gradient. The drainage divide is expected to migrate towards the part with the greatest χ-value and channel head elevation and the lowest gradient and relief. As indicated in the lower panel of the drainage divide stability metrics, drainage divide A is expected to migrate westward, while drainage divide B is expected to migrate eastward. The frequency bars and uncertainty plots in red represent eastward-flowing river catchments, whereas those in blue represent westward-flowing river catchments. The mean (μ) and standard deviation (σ) values of the channel head metrics are also coloured accordingly. Error bars (from top to bottom) represent one standard deviation, the 95% bootstrap confidence interval and one standard error.

clustering of knickpoints at similar χ locations in channels with similar substrates (e.g. Royden and Perron 2013). We observed no such clustering. This suggests that any response to Pliocene–Pleistocene base-level change, if it were once present, has migrated through the system or dissipated (Fig. 3).

A widely spaced NE–SW Hercynian fault pattern determines the form of many of the catchments and the orientation of many of the rivers of western Corsica (Fig. 4). However, despite the prevalence of these faults in Hercynian Corsica, the majority of large knickpoints are located north of northing 465000 (Fig. 3). South of northing 465000, the largest knickpoints occur in the headwaters of catchments where major faults are present and appear to be exploited by the river. The lithology mapped at the scale provided in Figure 3 does not seem to have an important role in dictating knickpoint location.

Tributary height above the mainstem

Using the novel approach of calculating the difference in height between the main stem channel and the associated tributaries, we found large differences in elevation across the island in tributary height compared with the equivalent height, at the same χ location, in the main stem channel (Fig. 4). Some of the tributaries, particularly in Alpine Corsica, have accumulated sediment-fill (Fig. 3) and these channels are below the main channel at the same χ-coordinate (Fig. 4). Tributaries in the northern regions that experienced extensive glaciation in the Würmian are perched high (*c.* 200–500 m) above the main channel in the region affected by the last glacial maximum (Fig. 4). Many of the NE–SW-oriented channels south of northing 465000 show high-elevation tributaries to the south of the main stem that are fault-controlled (e.g. catchment 15, Fig. 4).

We also calculated tributary differences using χ Q (Supplementary Figure S2) to try to isolate the extent to which the differences might be explained by precipitation gradients alone. There was no noticeable difference between the results.

Discussion

Our analysis of a range of topographic metrics and their relationship with lithological units, tectonic structures and climate suggests that the topographic state of Corsica is transient and adjusting. The current drainage divide is highly asymmetrical, located to the west in the north and to the east in the south (Fig. 2).

We deployed the Gilbert gradient metric and the difference in the χ coordinate across the divide to assess the stability of the drainage divide. Two of the recommended uncertainty monitors (i.e. one standard error, 95% bootstrap confidence interval and *t*-tests) revealed a statistically significant migration trend in Corsica (Supplementary Figure S1). The Gilbert and χ metrics showed the same migration direction (westward in the southern drainage divide and eastward in the northern drainage divide), which suggests that Corsica is undergoing a horizontal rearrangement of its drainage network and is not in a steady-state. It also suggests that the disequilibrium is strong: although Gilbert metrics are expected to reflect the dynamics of drainage divides by focusing on differences in topography near the divide, the χ-value has been shown to be highly sensitive to lithological variations and tectonic discontinuities along river profiles (Whipple *et al.* 2017; Forte and Whipple 2018; Zhou *et al.* 2022*a*, *b*), which abound in Corsica. However, the Gilbert metrics and χ disequilibrium at the divides agree on a regional scale (Fig. 5). The absence of obvious recent discrete river captures suggests that drainage expansion has happened primarily by continuous area gain/loss since the Pliocene, when the last discrete river captures are recorded in NE Corsica (Fellin *et al.* 2005*a*, *b*; Daníšík *et al.* 2012).

Knickpoints associated with transient signals should, by definition, separate a relict upstream area from a downstream region through which a wave of incision has propagated (Bishop *et al.* 2005; Crosby and Whipple 2006). The largest knickpoints in Corsica appear to be unrelated to sea-level or base-level changes – that is, they do not occur at a constant χ distance from the coastline, even where the lithology is constant (Fig. 3). Instead, the largest knickpoints are clustered in the NW, in the region most affected by Würmian glaciation (Figs 2, 3).

Given the absence of neotectonic activity on Corsica, we made a simple calculation of the adjustment timescale of the landscape. Mitchell and Yanites (2019), using a modified version of the analysis of Royden and Perron (2013), showed that the location of a migrating knickpoint in χ-space is simply $\chi_{kp} = Kt$, where K is an erodibility coefficient and t is the time elapsed from the originating time of the knickpoint if the slope exponent is assumed to be unity. The erodibility, K, can be estimated by dividing the erosion rate by k_{sn} (again assuming the slope exponent is unity). Note that, in this calculation, the same value of θ_{ref} needs to be used for the calculation of both χ and k_{sn}. The values of k_{sn} over the channel networks are of the order of 20 (Fig. 3) and, for erosion rates of 100 mm kyr^{-1} (at the slower end of erosion rate estimates since 7 Ma), we calculate knickpoints migrating 5 m in χ-space every 1 Myr. This slowing of erosion rates in the mid-Miocene could therefore be linked to profile concavities (e.g. in catchments 13 and 17, Fig. 3), but, again, these changes in channel steepness are not present in all catchments and cannot explain hanging valleys that occur at much shorter χ-distances. Early differential tectonic activity therefore has no clear impact on the location of knickpoints in either Hercynian or Alpine Corsica.

Drainage organization and planform morphology are strongly impacted by rainfall patterns. In Corsica, the mean annual rainfall is asymmetrical, with the highest rainfall related to regions of high relief (Fig. 2). This high precipitation is located over the expanding side of the drainage divide, potentially resulting in a top-down wave of erosion that is independent of headward knickpoint propagation. In the north, the situation is complicated by glacial pre-conditioning of the landscape with over-deepened valleys, as is evident from the difference in elevation between the tributaries and the main stem channel (Fig. 4).

Alpine Corsica is characterized by very few large knickpoints, except at the boundary with Hercynian Corsica. Given the known fluctuations in sea-level in the Mediterranean during the Pliocene and Pleistocene, this may be indicative of the rapid diffusion and equilibration of the channel profile within these primarily sedimentary (proto)lithologies. Lithology is therefore considered to be a third-order variable in knickpoint development in Corsica. However, geological structures are significant as linear zones of weakness that create local contrasts in erosional efficiency. For example, many of the large knickpoints in catchment 15 align in a NE–SW direction on the south side of the trunk stream (Figs 3, 4). We interpret this as the result of the drainage network exploiting the NE–SW basement fracture pattern inherited from the Hercynian Orogeny. This shows the importance of local structures on landscape morphology, even in locations with apparent lithological homogeneity (Fig. 4). Our knowledge of the strong NE–SW fabric across Hercynian Corsica allows us to identify the source of the documented knickpoints in catchment 15. Without this geological knowledge, these knickpoints, which occur within a uniform lithology, could have been interpreted as evidence of neotectonics.

The impact of climate on the landscape is clear. The topography in the NW was substantively affected by Pleistocene glaciation over-deepening the valleys and perching tributaries. This combination of early tectonic activity, which led to the growth of the mountainous landscape of Corsica, and climate change appears to be driving the transient, mobile form of the landscape evident today. Note that although tectonics can set signals in motion that may lead to drainage divide disequilibrium long after the cessation

of uplift (e.g. an asymmetrical drainage divide may move towards a more central position in a mountain range in response to the cessation of an uplift gradient), we do not believe that tectonics alone can explain the topography of Corsica and, in particular, the contrast between the two sections of the drainage divide, in the absence of a major tectonic discontinuity at the transition between these two sections.

Conclusions

Based on the statistical analyses of Gilbert and χ metrics, we identified two major directions of drainage divide migration in Corsica. The northern section of the drainage divide is currently migrating to the east, while the southern section is migrating westward. These patterns suggest that Corsica is in a transient state. The current direction of drainage divide motion mirrors the predicted trend required to ultimately reach a horizontal steady-state and drainage symmetry.

Hercynian Corsica has a higher density of knickpoints, especially in the region that experienced permanent glaciation in the Würmian (Fig. 2). Tributaries in this region are perched high above the main channel stem (Fig. 4). The modern drainage divide in the north is currently located in the region where glaciation was extensive and the valleys are over-deepened. The mean annual precipitation is highest east of the drainage divide in northern Corsica and indicates the direction that the divide is expanding towards.

The combination of tectonic and climatic pre-conditioning of the landscape has markedly influenced the form of the channel network and the topographic response in Corsica. A similar control may be evident elsewhere in regions that are devoid of strong tectonic signals (e.g. tectonically quiescent), but have experienced changes in climate.

Scientific editing by Sarah Boulton

Acknowledgements We thank the two anonymous reviewers for their very detailed and constructive comments that improved this paper.

Author contributions **RMH**: formal analysis (equal), methodology (equal), visualization (equal), writing – review and editing (equal); **CL**: investigation (equal), methodology (equal), writing – original draft (equal); **LAK**: conceptualization (equal), methodology (lead), supervision (lead), writing – original draft (equal), writing – review and editing (lead); **MA**: conceptualization (equal), formal analysis (lead), supervision (equal), writing – review and editing (equal); **SMM**: formal analysis (equal), visualization (equal), writing – original draft (equal), writing – review and editing (equal).

Funding C. Lavarini gratefully acknowledges support from a CAPES Brazilian PhD grant (BEX 13193–13–9).

Competing interests The authors declare that they have no known competing financial interests or personal relationships that could have appeared to influence the work reported in this paper.

Data availability The datasets generated during and/or analysed during the current study are available on request.

References

Baynes, E.R.C., Attal, M., Dugmore, A.J., Kirstein, L.A. and Whaler, K.A. 2015. Catastrophic impact of extreme flood events on the morphology and evolution of the lower Jökulsá á Fjöllum (northeast Iceland) during the Holocene. *Geomorphology*, **250**, 422–436, https://doi.org/10.1016/j.geomorph.2015.05.009

Bishop, P., Hoey, T.B., Jansen, J.D. and Artza, I.L. 2005. Knickpoint recession rate and catchment area: the case of uplifted rivers in Eastern Scotland. *Earth Surface Processes and Landforms*, **30**, 767–778, https://doi.org/10.1002/esp.1191

Brocard, G.Y., Willenbring, J.K., Miller, T.E. and Scatena, F.N. 2016. Relict landscape resistance to dissection by upstream migrating knickpoints. *Journal of Geophysical Research: Earth Surface*, **121**, 1182–1203, https://doi.org/10.1002/2015JF003678

Calvès, G., Toucanne, S. *et al.* 2013. Inferring denudation variations from the sediment record; an example of the last glacial cycle record of the Golo Basin and watershed, East Corsica, western Mediterranean Sea. *Basin Research*, **25**, 197–218, https://doi.org/10.1111/j.1365-2117.2012.00556.x

Cavazza, W., Zattin, M., Ventura, B. and Zuffa, G.G. 2001. Apatite fission-track analysis of Neogene exhumation in northern Corsica (France). *Terra Nova*, **13**, 51–57, https://doi.org/10.1046/j.1365-3121.2001.00316.x

Cavazza, W., DeCelles, P.G., Fellin, M.G. and Paganelli, L. 2007. The Miocene Saint–Florent Basin in northern Corsica: stratigraphy, sedimentology, and tectonic implications. *Basin Research*, **19**, 507–527, https://doi.org/10.1111/j.1365-2117.2007.00334.x

Condat, L. 2013. A direct algorithm for 1D total variation denoising. *IEEE Signal Processing Letters*, **20**, 1054–1057, https://doi.org/10.1109/LSP.2013.2278339

Crosby, B.T. and Whipple, K.X. 2006. Knickpoint initiation and distribution within fluvial networks: 236 waterfalls in the Waipaoa River, North Island, New Zealand. *Geomorphology*, **82**, 16–38, https://doi.org/10.1016/j.geomorph.2005.08.023

Daníšík, M., Kuhlemann, J., Dunkl, I., Evans, N.J., Székely, B. and Frisch, W. 2012. Survival of ancient landforms in a collisional setting as revealed by combined fission track and (U–Th)/He thermochronometry: a case study from Corsica (France). *Journal of Geology*, **120**, 155–173, https://doi.org/10.1086/663873

Danišík, M., Kuhlemann, J., Dunkl, I., Székely, B. and Frisch, W. 2007. Burial and exhumation of Corsica (France) in the light of fission track data. *Tectonics*, **26**, TC1001, https://doi.org/10.1029/2005TC001938

Devoti, R., D'Agostino, N. *et al.* 2017. A combined velocity field of the Mediterranean region. *Annals of Geophysics*, **60**, S0215, https://doi.org/10.4401/ag-7059

Duvall, A., Kirby, E. and Burbank, D. 2004. Tectonic and lithologic controls on bedrock channel profiles and processes in coastal California. *Journal of Geophysical Research: Earth Surface*, **109**, https://doi.org/10.1029/2003JF000086

Fellin, M.G., Picotti, V. and Zattin, M. 2005*a*. Neogene to Quaternary rifting and inversion in Corsica: retreat and collision in the western Mediterranean. *Tectonics*, **24**, https://doi.org/10.1029/2003TC001613

Fellin, M.G., Zattin, M., Picotti, V., Reiners, P.W. and Nicolescu, S. 2005*b*. Relief evolution in northern Corsica (western Mediterranean): constraints on uplift and erosion on long-term and short-term timescales. *Journal of Geophysical Research*, **110**, https://doi.org/10.1029/2004JF000167

Fick, S.E. and Hijmans, R.J. 2017. WorldClim 2: new 1 km spatial resolution climate surfaces for global land areas. *International Journal of Climatology*, **37**, 4302–4315, https://doi.org/10.1002/joc.5086

Finnegan, N.J., Schumer, R. and Finnegan, S. 2014. A signature of transience in rates of river incision into bedrock over timescales of 10^4–10^7 years. *Nature*, **505**, 391–394, https://doi.org/10.1038/nature12913

Flint, J.J. 1974. Stream gradient as a function of order, magnitude, and discharge. *Water Resources Research*, **10**, 969–973, https://doi.org/10.1029/WR010i005p00969

Forte, A.M. and Whipple, K.X. 2018. Criteria and tools for determining drainage divide stability. *Earth and Planetary Science Letters*, **493**, 102–117, https://doi.org/10.1016/j.epsl.2018.04.026

Gailleton, B., Mudd, S.M., Clubb, F.J., Peifer, D. and Hurst, M.D. 2019. A segmentation approach for the reproducible extraction and quantification of knickpoints from river long profiles. *Earth Surface Dynamics*, **7**, 211–230, https://doi.org/10.5194/esurf-7-211-2019

Gargani, J. 2004. Modelling of the erosion in the Rhone valley during the Messinian crisis (France). *Quaternary International*, **121**, 13–22, https://doi.org/10.1016/j.quaint.2004.01.020

Gilbert, G.K. 1877. *Report on the Geology of the Henry Mountains*. US Government Printing Office.

Goren, L., Fox, M. and Willett, S.D. 2014. Tectonics from fluvial topography using formal linear inversion: Theory and applications to the Inyo Mountains, California. *Journal of Geophysical Research (Earth Surface)*, **119**, 1651–1681, https://doi.org/10.1002/2014JF003079

Grieve, S.W.D., Mudd, S.M. and Hurst, M.D. 2016. How long is a hillslope? *Earth Surface Processes and Landforms*, **41**, 1039–1054, https://doi.org/10.1002/esp.3884

Harries, R.M., Aron, F. and Kirstein, L.A. 2023. Climate aridity delays morphological response of Andean river valleys to tectonic uplift. *Geomorphology*, **437**, 108804, https://doi.org/10.1016/j.geomorph.2023.108804

Kirby, E. and Whipple, K. 2012. Expression of active tectonics in erosional landscapes. *Journal of Structural Geology*, **44**, 54–75, https://doi.org/10.1016/j.jsg.2012.07.009

Kirstein, L.A., Carter, A. and Chen, Y.-G. 2014. Impacts of arc collision on small orogens: new insights from the Coastal Range detrital record, Taiwan. *Journal of the Geological Society, London*, **171**, 5–8, https://doi.org/10.1144/jgs2013-046

Knopf, E.B. 1924. Correlation of residual erosion surfaces in the eastern Appalachian Highlands. *Bulletin of the Geological Society of America*, **35**, 633–668, https://doi.org/10.1130/GSAB-35-633

Kuhlemann, J., Frisch, W., Székely, B., Dunkl, I., Daníšík, M. and Krumrei, I. 2005. Würmian maximum glaciation in Corsica: glacier extent, amplifying

paleorelief, and mesoscale climate. *Austrian Journal of Earth Science*, **97**, 68–81.

Kuhlemann, J., Van der Borg, K., Daníšík, M. and Frisch, W. 2007. Erosion rates on subalpine paleosurfaces in the western Mediterranean by in-situ 10Be concentrations in granites: implications for surface processes and long-term landscape evolution in Corsica (France). *International Journal of Earth Sciences*, **97**, 549–564, https://doi.org/10.1007/s00531-007-0169-z

Kuhlemann, J., Krumrei, I., Daníšík, M. and Van der Borg, K. 2009. Weathering of granite and granitic regolith in Corsica: short-term ^{10}Be versus long-term thermochronological constraints. *Geological Society, London, Special Publications*, **324**, 217–235, https://doi.org/10.1144/SP324.16

Mitchell, N.A. and Yanites, B.J. 2019. Spatially variable increase in rock uplift in the northern U.S. Cordillera recorded in the distribution of river knickpoints and incision depths. *Journal of Geophysical Research: Earth Surface*, **124**, 1238–1260, https://doi.org/10.1029/2018JF004880

Molliex, S., Jouet, G., Freslon, N., Bourlès, D.L., Authemayou, C., Moreau, J. and Rabineau, M. 2017. Controls on Holocene denudation rates in mountainous environments under Mediterranean climate. *Earth Surface Processes and Landforms*, **42**, 272–289, https://doi.org/10.1002/esp.3987

Morisawa, M.E. 1962. Quantitative geomorphology of some watersheds in the Appalachian Plateau. *GSA Bulletin*, **73**, 1025–1046, https://doi.org/10.1130/0016-7606(1962)73[1025:QGOSWI]2.0.CO;2

Mudd, S.M. 2017. Detection of transience in eroding landscapes. *Earth Surface Processes and Landforms*, **42**, 24–41, https://doi.org/10.1002/esp.3923

Mudd, S.M., Attal, M., Milodowski, D.T., Grieve, S.W. and Valters, D.A. 2014. A statistical framework to quantify spatial variation in channel gradients using the integral method of channel profile analysis. *Journal of Geophysical Research: Earth Surface*, **119**, 138–152, https://doi.org/10.1002/2013JF002981

Mudd, S.M., Clubb, F.J., Gailleton, B. and Hurst, M.D. 2018. How concave are river channels? *Earth Surface Dynamics*, **6**, 505–523, https://doi.org/10.5194/esurf-6-505-2018

Niemann, J.D., Gasparini, N.M., Tucker, G.E. and Bras, R.L. 2001. A quantitative evaluation of Playfair's law and its use in testing long-term stream erosion models. *Earth Surface Processes and Landforms*, **26**, 1317–1332, https://doi.org/10.1002/esp.272

Penck, A. 1905. Glacial features in the surface of the Alps. *The Journal of Geology*, **13**, 1–19, https://doi.org/10.1086/621202

Perron, J.T. and Royden, L. 2013. An integral approach to bedrock river profile analysis. *Earth Surface Processes and Landforms*, **38**, 570–576, https://doi.org/10.1002/esp.3302

Platt, J.P. 2007. From orogenic hinterlands to Mediterranean-style back-arc basins: a comparative analysis. *Journal of the Geological Society, London*, **164**, 297–311, https://doi.org/10.1144/0016-76492006-093

Rossi, P., Lahondère, J.C., Lluch, D., Loÿe-Pilot, M.D. and Jacquet, M. 1994. *Carte géologique de la France à 1/50000 Feuille 1103 Saint-Floren*. Bureau de Recherche Geologie et Mineralogie, Orléans, France.

Rovida, A., Locati, M., Camassi, R., Lolli, B. and Gasperini, P. 2020. The Italian earthquake catalogue CPTI15. *Bulletin of Earthquake Engineering*, **18**, 2953–2984, https://doi.org/10.1007/s10518-020-00818-y

Royden, L. and Perron, J.T. 2013. Solutions of the stream power equation and application to the evolution of river longitudinal profiles. *Journal of Geophysical Research: Earth Surface*, **118**, 497–518, https://doi.org/10.1002/jgrf.20031

Sømme, T.O., Piper, D.J., Deptuck, M.E. and Helland-Hansen, W. 2011. Linking onshore–offshore sediment dispersal in the Golo source-to-sink system (Corsica, France) during the late Quaternary. *Journal of Sedimentary Research*, **81**, 118–137, https://doi.org/10.2110/jsr.2011.11

Turco, E., Macchiavelli, C., Mazzoli, S., Schettino, A. and Pierantoni, P. 2012. Kinematic evolution of Alpine Corsica in the framework of Mediterranean mountain belts. *Tectonophysics*, **579**, 193–206, https://doi.org/10.1016/j.tecto.2012.05.010

Waelbroeck, C., Labeyrie, L., Michel, E., Duplessy, J.C., McManus, J.F., Lambeck, K. and Labracherie, M. 2002. Sea-level and deep water temperature changes derived from benthic foraminifera isotopic records. *Quaternary Science Reviews*, **21**, 295–305, https://doi.org/10.1016/S0277-3791(01)00101-9

Whipple, K.X. 2001. Fluvial landscape response time: how plausible is steady-state denudation? *American Journal of Science*, **301**, 313–325, https://doi.org/10.2475/ajs.301.4-5.313

Whipple, K.X., DiBiase, R.A., Ouimet, W.B. and Forte, A.M. 2017. Preservation or piracy: diagnosing low-relief, high-elevation surface formation mechanisms. *Geology*, **45**, 91–94, https://doi.org/10.1130/G38490.1

Willett, S.D., McCoy, S.W., Perron, J.T., Goren, L. and Chen, C.Y. 2014. Dynamic reorganization of river basins. *Science*, **343**, 1248765, https://doi.org/10.1126/science.1248765

Wobus, C.W., Whipple, K.X. *et al.* 2006*a*. Tectonics from topography: procedures, promise, and pitfalls. *GSA, Special Papers*, **398**, 55–74, https://doi.org/10.1130/2006.2398(04)

Wobus, C.W., Crosby, B.T. and Whipple, K.X. 2006*b*. Hanging valleys in fluvial systems: controls on occurrence and implications for landscape evolution. *Journal of Geophysical Research: Earth Surface*, **111**, https://doi.org/10.1029/2005JF000406

Zhou, C. and Tan, X. 2023. Quantifying the influence of asymmetric uplift, base level elevation, and erodibility on cross-divide difference. *Geomorphology*, **427**, 108634, https://doi.org/10.1016/j.geomorph.2023.108634

Zhou, C., Tan, X. *et al.* 2022*a*. Ongoing westward migration of drainage divides in eastern Tibet, quantified from topographic analysis. *Geomorphology*, **402**, 108123, https://doi.org/10.1016/j.geomorph.2022.108123

Zhou, C., Tan, X., Liu, Y. and Shi, F. 2022*b*. A cross-divide contrast index (C) for assessing controls on the main drainage divide stability of a mountain belt. *Geomorphology*, **398**, 108071, https://doi.org/10.1016/j.geomorph.2021.108071

Zhou, C., Tan, X., Liu, Y. and Shi, F. 2024. Quantifying the migration rate of drainage divides from high-resolution topographic data. *Earth Surface Dynamics*, **12**, 433–448, https://doi.org/10.5194/esurf-12-433-2024

Zondervan, J.R., Stokes, M., Boulton, S.J., Telfer, M.W. and Mather, A.E. 2020. Rock strength and structural controls on fluvial erodibility: implications for drainage divide mobility in a collisional mountain belt. *Earth and Planetary Science Letters*, **538**, 116221, https://doi.org/10.1016/j.epsl.2020.116221